RSC Advances

RSC Publishing

PAPER

View Article Online
View Journal | View Issue

Cite this: *RSC Advances*, 2013, **3**, 14088

Synthesis, crystal structure and bio-macromolecular interaction studies of pyridine-based thiosemicarbazone and its Ni(II) and Cu(II) complexes†

Arghya Basu,[a] Durairaj Thiyagarajan,[b] Chirantan Kar,[a] Aiyagari Ramesh*[b] and Gopal Das*[a]

Received 21st February 2013,
Accepted 20th May 2013

DOI: 10.1039/c3ra40904j

www.rsc.org/advances

A new pyridine-based heterocyclic thiosemicarbazone ligand and its Ni(II) and Cu(II) complexes have been synthesized and characterized by structural, analytical and spectral methods. The mono-deprotonated anionic form of the ligand coordinates *via* NNS donor atoms to yield an octahedral Ni(II) complex and distorted square planar Cu(II) complex. UV-visible and fluorescence-based spectroscopic techniques revealed that both metal complexes interact with double stranded DNA *via* intercalation. A comparative assessment indicated that the Ni(II) complex displayed superior DNA binding. The interaction of these compounds with bovine serum albumin (BSA) suggested that the ligand and its Cu(II) complex quenched the intrinsic fluorescence of BSA in a static quenching process, whereas for the Ni(II) complex, fluorescence quenching of BSA was a combination of both static and collision/dynamic quenching processes. The quenching of the fluorescence of BSA is owing to energy transfer from the tryptophan residues of BSA to the compounds bound to BSA. Cytotoxicity tests based on the standard MTT assay revealed that the Cu(II) complex displayed prominent anti-proliferative activity against HeLa cells.

Introduction

Thiosemicarbazones constitute a class of ligand which holds considerable interest to medicinal chemists owing to their therapeutic potential.[1,2] Over the last few decades, thiosemicarbazones and their transition metal complexes have received substantial attention not only due to their coordination behavior,[2] but also their valuable pharmacological properties, such as antitumor, antibacterial, antiviral and antimalarial activities.[3–14] Additionally, thiosemicarbazones can also undergo ring closure processes through the action of bases, acids or oxidants.[15] Recently, we have shown that oxidative cyclization of thiosemicarbazone can be used for selective chemodosimetric sensing of Cu(II) ions.[15h]

With regard to biological activity, metal complexes of heterocyclic thiosemicarbazones exhibit more promising results compared to other non heterocyclic thiosemicarbazones.[16] Many heterocyclic thiosemicarbazones, such as triapine[4e] or marboran,[4b–d] are already employed in medical practices. Recently, Natarajan and coworkers have shown that metal complexes derived from thiosemicarbazones with a 2-oxoquinoline heterocycle unit exhibit outstanding DNA/protein binding and antitumor activities, and this improved biological activity could be attributed to the presence of the heterocycles present in the thiosemicarbazones.[16–18]

The development of transition metal complexes with DNA binding abilities has been an active area of research due to their potential applications as metallo-drugs, tools for molecular biology, a regulator of gene expression and others. Recently, substantial numbers of studies have been carried out on transition metal complexes for their ability to mediate oxidative damage to nucleobases and/or to the 2-deoxyribose moiety in the presence of an oxidizing or reducing agent, light or metal centers with potential redox activity.[19] It is well documented in the literature that metal complexes interact with DNA in a non-covalent fashion, such as electrostatic binding, groove binding and intercalation. The development of metal complexes with intercalation or a groove binding mode of interaction with DNA are more promising[19e] compared to those metal complexes which interact with DNA through weak electrostatic interactions.

In the context of therapeutic applications of a potential drug, it is pertinent to investigate the protein binding levels of the drug, especially to serum albumins, as these proteins may influence the metallo-pharmaceutical pharmacokinetics and structure–activity relationships.[20] Bovine serum albumin (BSA)

[a]*Department of Chemistry, Indian Institute of Technology, Guwahati. E-mail: gdas@iitg.ernet.in; Fax: +91-361-2582349; Tel: +91-361-2582313*
[b]*Department of Biotechnology, Indian Institute of Technology, Guwahati. E-mail: aramesh@iitg.ernet.in; Fax: +91-361-258-2249; Tel: +91-361-258-2205*

† Electronic supplementary information (ESI) available: Compound characterization spectra, crystallographic files in CIF format, additional crystallographic data, characterization data. CCDC 905339 905341 905340. For ESI and crystallographic data in CIF or other electronic format see DOI: 10.1039/c3ra40904j

has been widely used as a model protein to study drug interactions due to its structural resemblance to human serum albumin (HSA). Additionally, serum albumins are also identified as major transport proteins in blood plasma for many compounds, such as fatty acids, which are otherwise insoluble in plasma, hormones, bilirubin and many drugs. These facts reiterate the importance of studying the interaction behavior of potential drugs with BSA protein whilst assessing their biological properties. In this context, we have previously reported protein sensing and detailed interaction studies with structurally diverse amphiphilic organic ligands.[21]

Considering the above objectives, herein, we report the synthesis and characterization of a newly synthesized pyridine-based heterocyclic thiosemicarbazone ligand and its mononuclear Cu(II) and Ni(II) complexes and demonstrate their potential biological activity. The ligand and its complexes are structurally characterized by single-crystal X-ray crystallography. The study highlights the DNA and protein binding characteristics of the test compounds as well as their antiproliferative effects on human cervical carcinoma HeLa cell lines.

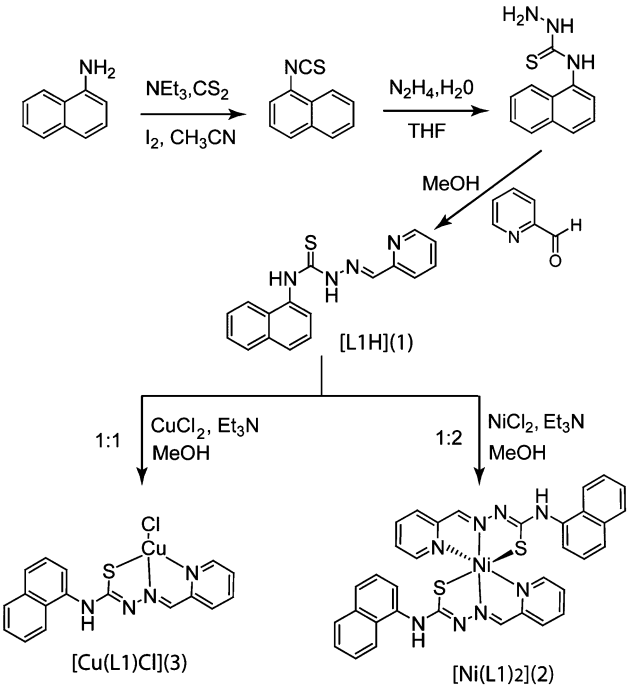

Scheme 1 Synthesis of the ligand LH and its Cu(II) and Ni(II) complexes.

Experimental

Materials

All reagents were obtained from commercial sources and used as received. Solvents were freshly distilled following standard procedures. Napthylamine, carbondisulphide, triethylamine, iodine, dimethyl sulfoxide (DMSO), hydrated $CuCl_2$ and hydrated $NiCl_2$ were purchased from Merck, India and used as received. BSA was purchased from Fluka, Germany and was used as supplied. Calf thymus DNA (CT-DNA), ethidium bromide (EtBr), Dulbecco's Modified Eagle Medium (DMEM), trypsin-EDTA and 3-(4,5-dimethyl-2-thiazolyl)-2,5-diphenyl-2*H*-tetrazolium bromide (MTT) were procured from Sigma Aldrich, USA and plasmid DNA pUC18 was purchased from Bangalore Genei, India. Fetal calf serum (FCS) was procured from PAA Laboratories, USA. The synthetic route for the ligand and its complexes is shown in Scheme 1.

Synthesis and characterization

Synthesis of 1-naphthylisothiocyanate. This compound was synthesized by a previously reported literature procedure.[26]

Synthesis of 4-(1-naphthyl)-3-thiosemicarbazide. In a 100 ml round bottom flask, 1.85 g of naphthyl isothiocyanate (10 mmol) was dissolved in 50 mL of dry THF. Then, excess hydrazine hydrate (30 mmol, 0.9 ml) was added to the solution at once. After stirring under ice cold conditions for 2 h, the precipitate was filtered and washed with 5 mL of diethyl ether three times. A colorless solid was obtained after drying the precipitate in a vacuum over silica gel. Yield 85%.

Synthesis of pyridine-2-carboxaldehyde-4-(1-naphthyl)-3-thiosemicarbazone [LH] (1). The compound LH was prepared by the condensation of pyridine-2-carboxyaldehyde and 4-(1-naphthyl)-3-thiosemicarbazide. Pyridine-2-carboxyaldehyde (0.560 mL, 5 mmol) was added over a solution of 4-(1-naphthyl)-3-thiosemicarbazide (1.085 g, 5 mmol) in ethanol (15 mL). The light yellow solution was stirred at room temperature for 3 h. The white solid formed was collected by filtration, washed thoroughly with ethanol and diethyl ether and dried *in vacuo*. Yield 87%. ^{1}H NMR (400 MHz, DMSO-d_6) δ-12.18(s, 1H) 10.59(s, 1H), 8.60(s, 1H), 8.5(d, 1H), 8.27(s, 1H), 7.99(m, 1H), 7.9–7.8(m, 3H), 7.6–7.5(m, 4H), 7.4(m, 1H), ^{13}C NMR (100 MHz, DMSO-d_6) δ- 178.35, 153.38, 149.36, 143.05, 136.50, 135.65, 133.75, 130.61, 128.06, 127.14, 126.58, 126.18, 126.12, 125.51, 124.23, 123.45, 120.67 IR (KBr, cm^{-1}): 3348(N–H), 1540(C=N, sym), 1504 (C=S) and 780(C=S, asym) ESI† mass calcd for 322.4. [M + H$^+$]; found 322.4 [M + H$^+$]. MP 194 °C.

Synthesis of [Ni(L)$_2$] (2). The complex $Ni(L)_2$ was synthesized by stirring an ethanolic solution of $NiCl_2{\cdot}6H_2O$ (0.24 g, 1 mmol, 10 mL) and LH (0.64 g, 2.5 mmol, 25 mL) in the presence of triethylamine (1 ml). The stirring was continued for 5 h. The yellowish green precipitated complex was collected by filtration, washed with a cold 1 : 1 EtOH and H_2O mixture to remove any impurities and finally dried in vacuum over silica gel. It is important to mention here, we have also tried to prepare a 1 : 1 Ni(II)-thiosemicarbazone complex by varying the metal–ligand stoichiometry but in all the cases, a 1 : 2 (metal : ligand) complex was obtained, which was confirmed by single crystal X-ray diffraction and elemental analysis. Yield 62%. Calc. for $C_{38}H_{36}N_9NiOS_2$: C, 60.25; H, 4.79; N, 16.64; S, 8.47 Found: C, 59.94; H, 4.49; N, 16.75; S, 8.36, IR (KBr, cm^{-1}): 3348(N–H), 1674(C=N), 1597(C=S) and 772(C=S, asym), MP 264 °C. μ_{eff} (300 K): 2.98 μ_B, Λ_M (S mol^{-1} cm^2): 0.66.

Synthesis of [Cu(L)Cl] (3). The complex Cu(L)Cl was synthesized by refluxing an equimolar amount of ethanolic solutions of $CuCl_2{\cdot}2H_2O$ (0.085 g, 0.5 mmol) and the ligand LH

(0.115 gm, 0.5 mmol) in the presence of Et_3N (0.5 ml) for 2 h (Scheme 1). The brownish red precipitated complex was collected by filtration, washed with cold ethanol to remove any unreacted starting materials and impurities and finally dried in a vacuum over silica gel. Yield 62%. Calc. for $C_{17}H_{13}ClCuN_4S$: C, 50.49; H, 3.24; N, 13.86; S, 7.93 Found: C, 50.54; H, 3.19; N, 13.75; S, 8.06, IR (KBr, cm^{-1}): 3348(N–H), 1601(C=N), 1477(C=S) and 764(C=S, asym) MP 205 °C. μ_{eff} (300 K): 1.72 μ_B, Λ_M (S mol^{-1} cm^2): 1.25.

Instruments

IR spectra were recorded on a Perkin-Elmer-Spectrum One FT-IR spectrometer with KBr disks in the range 4000–400 cm^{-1}. UV-visible and fluorescence spectra were recorded with a Perkin-Elmer Lambda-25 and FlouroMax-3, HORIBA spectro-fluorometer, respectively. ^1H NMR spectra were recorded at 400 MHz and ^{13}C NMR spectra were recorded at 100 MHz using a Varian AS400 spectrometer. Chemical shifts were recorded in parts per million (ppm) on the scale solvent peak as a reference. Elemental analyses were obtained from a Perkin-Elmer Series II Analyzer. The magnetic moments of the complexes were measured on a Cambridge Magnetic Balance. Solution electrical conductivity was measured using a Systronic 305 conductivity bridge in a 5% aqueous DMSO solution. ESI-MS spectra were recorded in a WATERS LC-MS/MS system, Q-Tof Premier in the Central Instrument Facility (CIF) of IIT Guwahati.

X-ray crystallography

Intensity data were collected using a Bruker SMART APEX-II CCD diffractometer equipped with fine focus 1.75 kW sealed tube Mo–Kα radiation (λ) 0.71073 (Å) at 298 K, with increasing ω (width of 0.3° per frame) at a scan speed of 5 s per frame. The SMART software was used for the data acquisition. Data integration and reduction were performed with the SAINT and XPREP software.[22] Multi-scan empirical absorption corrections were applied to the data using the program SADABS.[23] The structures were solved by direct methods using SHELXS-97[24a] and refined with full-matrix least squares on F^2 using the SHELXL-97[24b] program package. All non-hydrogen atoms were refined anisotropically. The hydrogen atoms attached to all carbon and nitrogen atoms were geometrically fixed and the positional and temperature factors were refined isotropically. Structural illustrations have been drawn with MERCURY[25] for Windows. A summary of the crystal data and relevant refinement parameters are given in Table 1. CCDC 905339 (**1**), 905340 (**3**) and 905341 (**2**) contain the supplementary crystallographic data for this paper.

DNA binding studies

UV-visible spectroscopy

The DNA interaction experiments were carried out in sterile phosphate buffered saline (PBS) whose pH was adjusted to 7.4. For the calf-thymus DNA, a molar extinction coefficient value of 6600 M^{-1} cm^{-1} at 260 nm was used to determine the DNA molarity.[17] Stock solutions of the test compounds were prepared in DMSO and diluted to the appropriate concentrations in PBS prior to the experiments, while a stock solution of CT-DNA was prepared in sterile PBS. For the UV-visible absorption titration experiments, 30 μM of each test compound was interacted with various concentrations of CT DNA (3 μM–30 μM). In these experiments, the DNA solution was added drop-wise to the test compound, mixed gently and then the absorbance of the solution was measured. Control samples consisting of only the DNA solution or the test compounds were also included in the experiments.

Table 1 Crystal parameters and refinement data

Compound	[LH] (**1**)	[Ni(L)$_2$] (**2**)	[Cu(L)Cl] (**3**)
Formula	$C_{17}H_{14}N_4S$	$C_{37}H_{33}N_9NiOS_2$	$C_{17}H_{13}ClCuN_4S$
Formula weight	306.39	742.55	404.38
Crystal system	Monoclinic	Monoclinic	Monoclinic
Space group	P 21	P 21	P 21/c
a/Å	9.5334(4)	9.0267(10)	7.5413(4)
b/Å	6.4275(2)	33.436(3)	13.9846(8)
c/Å	13.0570(5)	12.2036(11)	15.6339(9)
β (°)	108.293(2)	100.916(6)	101.290(3)
V (Å)	759.65(5)	3616.6(6)	1616.88(16)
Z	2	4	4
T/K	298(2)	298(2)	298(2)
μ/cm^{-1}	0.214	0.696	1.651
dcal (g cm^{-3})	1.339	1.364	1.661
Cryst dimens (mm^3)	0.28 × 0.26 × 0.22	0.42 × 0.34 × 0.29	0.26 × 0.19 × 0.17
no. of reflns collected	3313	17 936	3978
no. of unique reflns	2999	16 528	2648
no. of params	207	905	221
R_1; *wR*2 ($I > 2\sigma(I)$)	0.0444, 0.1197	0.0879, 0.2039	0.0306, 0.0721
R(int)	0.0786	0.102	0.0719
GOF (F^2)	0.909	0.857	0.912
Flack prameter	−0.15(7)	0.009(6)	—
CCDC NO.	905339	905341	905340

Fluorescence spectroscopy

For the fluorescence emission spectroscopic measurements, 30 μM of the test compounds were interacted with varying CT-DNA concentrations (6 μM–30 μM). As mentioned before, the emission titration experiments were performed by the drop-wise addition of a CT-DNA solution to the test compounds followed by gentle mixing and then the fluorescence emission spectra of the samples were recorded in a scanning mode from 335 nm to 600 nm by setting the excitation wavelength at 320 nm in a spectrofluorometer. Control samples consisting of only the DNA solution or the test compounds were also included in the experiments.

Ethidium bromide displacement experiment

Initially, a 3 μM CT-DNA solution (taken in sterile PBS, pH 7.4) was incubated with a 0.5 μM EtBr solution for 1 h at 37 °C in an amber colored microcentrifuge tube. Subsequently, varying concentrations of the test compounds (0.6 μM–3 μM) were gradually dispensed into the tubes, incubated for 5 min at room temperature and then the fluorescence emission spectra of the samples were recorded in a scanning mode from 530 nm to 720 nm by setting the excitation wavelength at 515 nm in a spectrofluorometer. Emission spectra were also recorded for DNA-bound EtBr alone in the absence of the test compounds.

Plasmid cleavage experiment

To determine the DNA cleavage activity of the compounds, purified pUC18 plasmid DNA (60 μM) was taken in a 5 mM Tris-HCl–50 mM NaCl buffer and incubated with varying concentrations of the test compounds (60 μM and 180 μM) for 1 h and 2 h. Control samples were also included, which consisted of pUC18 plasmid DNA treated with equivalent concentrations of the Cu(II) and Ni(II) salts and DMSO separately. Following incubation for the specified time, a loading buffer (0.05% bromophenol blue, 50% glycerol and 2 mM EDTA) was added to each reaction tube. Subsequently, the samples were subjected to agarose gel (0.8%) electrophoresis followed by staining the gel with an EtBr solution and the DNA bands were visualized in a gel documentation system.

BSA interaction studies

A 10 mM phosphate buffer of pH 7.4 was prepared in double-distilled water for all the experiments. A stock solution of BSA (10 μM) was prepared in an aqueous solution of a 10 mM phosphate buffer of pH 7.4, while stock solutions of the test compounds were prepared in dimethyl sulfoxide (DMSO). In a 1.0 mL aqueous buffer solution of BSA (1 μM), different concentrations of compounds were added (0 to 40 μM), so that the total volume of DMSO did not exceed 15%. The presence of 15% DMSO induces no major BSA structural changes.[21a] Each solution was mixed thoroughly before the spectral measurements at room temperature (RT). For the fluorescence resonance energy transfer (FRET) experiments, the concentration of BSA and the ligands were kept at 3 μM. The absorption spectra were recorded at 298 K in the range of 200–450 nm. Fluorescence measurements were taken at 298 K with a slit width of 2 nm. An excitation wavelength of 295 nm was applied to selectively excite the tryptophan residues in the protein. The background intensities of the buffer blanks were subtracted from each sample spectrum to cancel out any contribution due to the solvent.

Cytotoxicity assay

The cytotoxicity assay for the test compounds was performed on human cervical carcinoma (HeLa) cell lines by a standard MTT assay following the manufacturer's instructions (Sigma-Aldrich, MO, USA). HeLa cells were initially propagated in Dulbecco's Modified Eagle Medium (DMEM) supplemented with 10% fetal calf serum (FCS). Subsequently, HeLa cells were seeded in a 96 well tissue culture plate (10^4 cells well^{-1}) and varying concentrations of the test compounds (15 μM, 30 μM and 60 μM) constituted in DMEM devoid of FCS were added to the cells. The cells were incubated for a period of 24 h in a CO_2 incubator with 5% CO_2. Control samples consisting of the cells alone and DMSO-treated cells (solvent control) were also included in each assay. Following incubation, the growth media was aspirated, a fresh DMEM-containing MTT solution was added and the plate was incubated for 4 h at 37 °C. Subsequently, the supernatant was gently removed and the insoluble colored formazan product was solubilized in DMSO and measured spectrophotometrically at 550 nm in a mutiplate reader (Perkin Elmer, USA). Every sample in the MTT assay was taken in six sets. To determine the statistical significance of the results, the obtained data were subjected to analysis of the variance (ANOVA) using a Sigma plot.

Results and discussion

Crystal structure of [LH] (1)

The structure of LH was established accurately by X-ray diffraction of single crystals. Light yellow block shaped crystals of the ligand were grown by slow driven crystallization from a saturated solution of DMSO. It crystallized in the space group $P2_1$ with $Z = 2$. The molecular structure of LH along with the atom numbering scheme is depicted in Fig. 1. The detail structural analysis of LH shows the thiosemicarbazone ligand exists in its thione form, confirmed by the presence of hydrazinic hydrogen. The sulfur atom S1 and the hydrazone nitrogen N3 are in the *E* configuration with respect to the C11–N2 bond. This lower energy configuration helps the formation

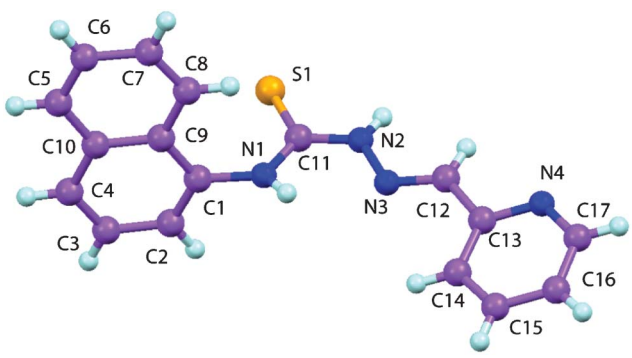

Fig. 1 Molecular structure of LH with an atom numbering scheme.

of N2–H···N4 hydrogen bond interactions, which subsequently form a 1D hydrogen-bonding chain along the crystallographic *b* axis (Fig. S8, ESI†). Probably, the presence of the strong H-bond accepting pyridine N(4) nitrogen prevents the formation of centrosymmetric dimeric interactions through N–H···S hydrogen bonds, which is very common for a thiosemicarbazone type of ligand. The N2–N3 (1.377(3) Å) and N2–C11 (1.350(3) Å) bond distances in LH are in between the ideal values corresponding single [N–N, 1.45 Å; C–N, 1.47 Å] and double bonds [N=N, 1.25 Å, C=N, 1.28 Å], as evident for an extended π-delocalization throughout the thiosemicarbazone function. The elaborate 3D network of LH is mainly governed by the combination of H-bonding and C–H···π interactions.

Crystal structure of [Ni(L)$_2$·DMF] (2)

The isolated yellowish green Ni(II) complex was crystallized by isothermal slow evaporation of a saturated DMF solution. It crystallized in the space group $P2_1$ with $Z = 4$. The molecular structure of Ni(L)$_2$ along with the atom numbering scheme is depicted in Fig. 2 and selected bond lengths and bond angles are given in Table 2 and Table 3. The asymmetric unit is composed of two symmetry-independent octahedral complex molecules along with two crystallized DMF molecules exhibiting conformational isomorphism. Their occurrence is generally controlled by both kinetic and thermodynamic crystal stability because these factors are mostly considered to be the consequences of interrupted crystallization. Both complexes in the asymmetric unit are almost identical, therefore, in this crystallographic description section, we only consider the first complex unit.

The two deprotonated S,N,N–tridentate ligands chelate the nickel atom, giving a distorted octahedral geometry around the nickel centre. Moreover, the elongated C–S bonds in the complex molecule compared to the free ligand also indicate that the ligands are bound to nickel in the thiolate form (Table 2). The negative charge of the deprotonated ligand is fully delocalized along the thiosemicarbazone moiety, confirmed by a detailed bond length comparison of the thiosemicarbazone functions of the coordinated ligands (Table 2). Interestingly, two symmetry independent complex molecules in the asymmetric unit form dimeric interaction *via* two N5–H···N10 hydrogen bonds, forming an $R^2_2(8)$ ring motif (Fig. S9, ESI†). The free DMF solvents are stabilized by the hydrogen bonding (N–H···O and C–H···O) and C–H···π interactions with the complex molecules.

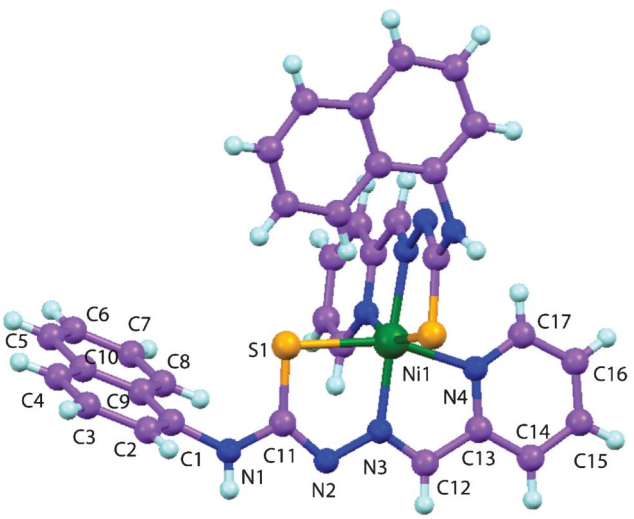

Fig. 2 Molecular structure of Ni(L)$_2$ with an atom numbering scheme. The other unit and solvent (DMF) molecules are omitted for clarity.

Table 2 Comparison of selected bond lengths (Å) and bond angles (°) of LH, [Ni(L)$_2$] and [Cu(L)Cl]

	[LH] (**1**)	[Ni(L)$_2$] (**2**)	[Cu(L)Cl](3)
N1–C11	1.350(3)	1.387(1)	1.362(3)
C11–N2	1.350(3)	1.322(2)	1.313(2)
N2–N3	1.377(3)	1.365(1)	1.374(2)
N3–C12	1.278(3)	1.279(2)	1.284(3)
C11–S1	1.670(2)	1.738(1)	1.745(2)
N4–C13–C12	114.2(2)	115(1)	114.3(2)
C12–N3–N2	114.3(2)	116.6(9)	119.0(2)
N2–C11–S1	119.4(1)	128.1(9)	125.9(2)

Crystal structure of [Cu(L)Cl] (3)

The isolated brownish red Cu(II) complex was crystallized by vapor diffusion of Et_2O into a 2 : 1 $CHCl_3$: DMF solution. The complex crystallized into a monoclinic space group $P2_1/c$ with $Z = 4$. The molecular structure of Cu(L)Cl along with the atom numbering scheme is depicted in Fig. 3 and significant structural parameters are given in Table 2 and Table 3. The molecular structure of the complex shows that the mono-negative thiosemicarbazone ligand (L) binds to the Cu(II) center *via* N,N,S-donor atoms, resulting in two five membered chelate rings. The fourth coordination site around Cu(II) is occupied by a chloride anion, forming a distorted square planer complex. The bonding parameters are in good agreement with the coordinating pattern of a thiosemicarbazone *via* the thiolate form. While coordinating in their iminothiolate forms, the negative charges generated by deprotonation are effectively delocalized in the C–N–N–C system, as shown by the intermediate C12–N3 [1.284 Å], N3–N2 [1.374 Å] and N2–C11 [1.313 Å] bond distances. The bond angles Cl1–Cu–S1 97.74(2),

Table 3 Metal–ligand bond lengths (Å) and angles (°) for the Ni(L)$_2$ and Cu(L)Cl complexes

Ni(L)$_2$			
S1–Ni1	2.419(4)	S2–Ni1	2.403(3)
N3–Ni1	2.028(8)	N7–Ni1	2.04(1)
N4–Ni1	2.11(1)	N8–Ni1	2.13(1)
S1–Ni1–S2	96.6(1)	S2–Ni1–N3	104.1(3)
S1–Ni1–N3	80.1(3)	S2–Ni1–N4	89.7(3)
S1–Ni1–N8	94.4(3)	S2–Ni1–N7	80.3(3)
S1–Ni1–N7	103.4(3)	N7–Ni1–N8	79.1(4)
N3–Ni1–N8	96.0(4)	N7–Ni1–N4	97.1(4)
N3–Ni1–N4	79.2(4)	N8–Ni1–N4	86.4(4)
Cu(L)Cl			
S1–Cu1	2.2562(7)	N3–Cu1	1.970(2)
Cl1–Cu1	2.2076(6)	N4–Cu1	2.2027(2)
Cl1–Cu1–S1	97.74(2)	S1–Cu1–N3	83.29(5)
Cl1–Cu1–N4	98.34(5)	N3–Cu1–N4	80.69(6)

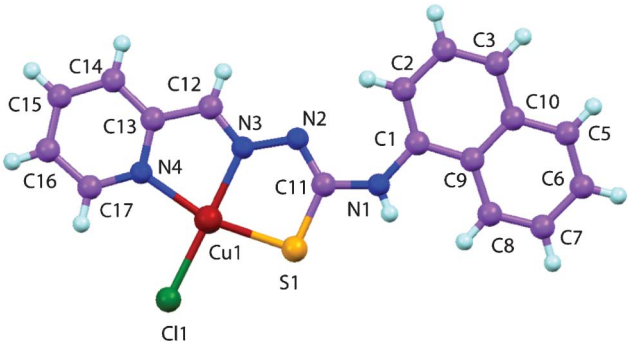

Fig. 3 Molecular structure of Cu(L)Cl with an atom numbering scheme.

Cl1–Cu–N4 98.34(5), N3–Cu1–S1 83.295 and N3–Cu1–N4 80.69(6) illustrate that the complex is slightly distorted from the square planar geometry (τ_4 = 0.12). In this complex, two chelate rings are formed, which are almost planar with a dihedral angle separation of 1.79°, the second chelate ring being Cu1–N4–C13–C12–N3. A similar type of distorted square planar Cu(II) thiosemicarbazone complex (τ_4 = 0.14) with a coordinated linear isothiocyanate counter anion was previously reported by Kurup and coworkers, whereas in the case of the chloride counter anion, they obtained a chloride bridged centrosymmetric dimeric Cu(II) complex.[27] Interestingly, in the present study, hydrogen bonding interactions were not observed in the Cu(II) complex, whereas the 3D network of Cu(L)Cl was mainly controlled by π···π stacking interactions (Fig. S11, ESI†).

DNA binding studies

UV-visible spectroscopic studies

Absorption spectroscopy is a common tool to decipher the mode of binding of test compounds to DNA. It is quite well established that the binding of a compound to DNA may typically lead to hypochromism, which can be largely attributed to intercalation through stacking between the planar aromatic chromophore of the test compound and the bases present in DNA.[28] In the present study, UV-visible absorption spectroscopy of the complexes indicated that the absorbance maxima of compounds **1**, **2** and **3** were 317 nm, 432 nm and 459 nm, respectively. The UV-visible absorption spectra of compounds **1–3** (30 μM) with increasing concentrations of CT DNA (3 μM–30 μM) are indicated in Fig. 4. As observed in Fig. 4A, the interaction of compound **1** with increasing DNA concentrations resulted in marginal hypochromism of 6.43% at the absorbance maxima (317 nm) of the compound. In contrast to the ligand alone, the metal complexes revealed a distinctly higher hypochromic shift of the absorption bands upon interaction with incremental concentrations of DNA, indicating that the binding strength of the metal complexes is superior to that of the free ligand. For instance, the extent of the hypochromism for compound **2** was around 25% at 432 nm, whereas compound **3** exhibited a hypochromic shift of around 18% at 459 nm. The observed hypochromic shifts for compound **2** and **3** perhaps indicate an intercalative mode of binding with CT-DNA.[28] The UV-visible spectra of compound **2** and **3** (Fig. 4B and 4C) also reveal that the binding of the complexes to CT-DNA led to an isosbestic spectral change with an isosbestic point at 293 nm. It may also be mentioned here that the binding of increasing concentrations of CT-DNA lead to negligible shifts in the absorption maxima for all the compounds. From the comparative measurements of the hypochromic shifts following binding with CT-DNA, it can be assumed that compound **2** has the highest propensity to interact with DNA. The binding constants (K_b) for compounds **1**, **2** and **3** were determined from the UV spectroscopic studies by monitoring the change in absorbance at 260 nm on increasing the concentration of the DNA and calculating the ratio of the slope to the *y* intercept in the plots of [DNA]/($\varepsilon_a - \varepsilon_f$) *versus* [DNA][6h,17] (insets in Fig. 4). The values for the binding constants for compounds **1**, **2** and **3** were 1.37 × 10^5 M^{-1}, 1.15 × 10^5 M^{-1} and 1.13 × 10^5 M^{-1}, respectively. In the present study, the binding constant for the Ni-complex (compound **2**) was comparatively lower than the binding constants reported earlier for analogous Ni(II)

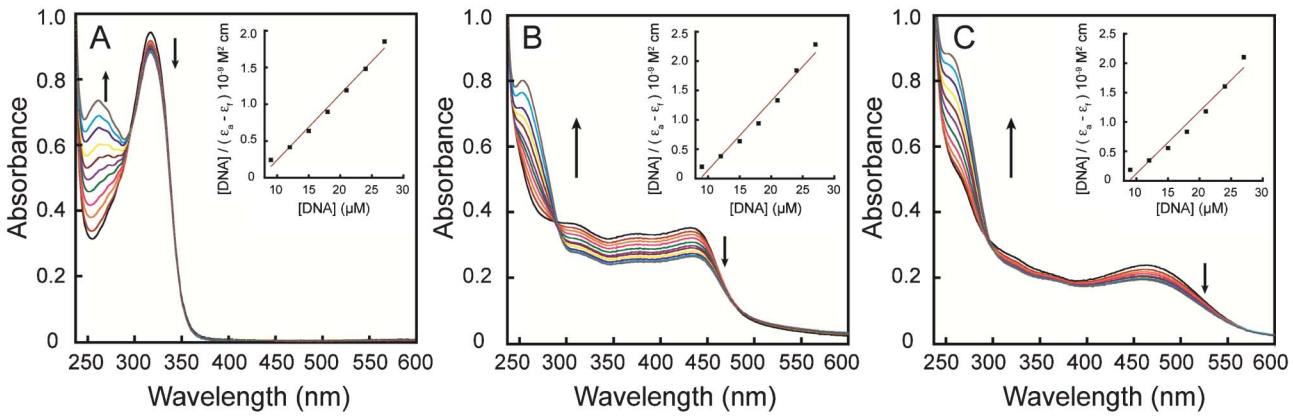

Fig. 4 Absorbance titration spectra of (A) compound **1** (B) compound **2** (C) compound **3** with various concentrations (6 μM–30 μM) of CT-DNA in PBS pH 7.4. Inset indicates binding isotherms with CT-DNA.

thiosemicarbazone complexes,[6h] whereas in the case of the Cu-complex (compound **3**), the calculated binding constant was observed to be higher than similar Cu(II) semicarbazone complexes.[17]

Fluorescence experiment

To acquire an insight into the mode of binding of the compounds to CT-DNA, we performed fluorescence titration experiments. As evident from Fig. S12A (ESI†), when compound **1** was excited at 320 nm, a fluorescence emission peak was observed at 439 nm. It was also observed that the fluorescence of compound **1** was enhanced progressively upon interaction with incremental concentrations of CT-DNA (6 μM–30 μM). At the highest CT-DNA concentration of 30 μM, the fluorescence emission intensity of compound **1** was nearly doubled. In the case of the Ni(II)-complex (compound **2**), the enhancement in the fluorescence emission intensity of the compound with increasing concentrations of CT-DNA was quite substantial, resulting in a nearly four-fold increase upon interaction with 30 μM CT-DNA (Fig. 12B, ESI†). At this concentration of CT-DNA, it was also noted that the fluorescence emission maximum changed considerably from 457 nm for the compound alone to 436 nm following its interaction with CT-DNA. For compound **3**, the increase in the fluorescence intensity upon its interaction with CT-DNA was minimal and was not accompanied by any peak shift in the emission maximum (Fig. S12C, ESI†). The increase in the fluorescence intensity of the ligand alone as well as the metal complex upon its interaction with the DNA suggests that the compounds perhaps gain access into the hydrophobic core of the DNA bases upon intercalation, which may result in enhanced fluorescence.[28,29a,30] On the basis of fluorescence enhancement and the large shift in the fluorescence maxima, it is quite evident that compound **2** interacts strongly with CT-DNA, in comparison to compound **1** or compound **3**.

Ethidium bromide (EB) displacement assay

The binding of compounds **1–3** to DNA *via* intercalation was further verified by an EtBr displacement assay (Fig. S13, ESI†). A systematic decrease in the fluorescence emission intensity of DNA-bound EtBr on increasing the compound concentration was observed for all the compounds. At the highest compound concentration, the emission band of DNA-bound EtBr at 603 nm revealed a moderate hypochromic shift of the initial fluorescence emission intensity (Fig. S13 A–C, ESI†). This reduction in the fluorescence of DNA-bound EtBr suggests that compounds **1–3** compete for the binding site on DNA, which results in the displacement of EtBr, as reported in earlier studies.[17,31]

The quenching of the EtBr fluorescence by the compounds was analyzed by the standard Stern–Volmer equation which may be represented as:

$$F_0/F = K_q[Q] + 1 \quad (1)$$

where F_0 is the initial DNA-bound EtBr emission intensity, F is fluorescence intensity in the presence of a quencher, K_q represents the quenching constant, and [Q] is the concentration of the quencher. The slope of the plot of F_0/F *versus* [Q] provides a measure of the quenching constant K_q of the compounds.[17,29b,31] The plot of F_0/F *versus* [Q] for compounds **1–3** is shown in Fig. S13D (ESI†) and it is quite evident that the plot for each compound is consistent with the expected linear pattern of a characteristic Stern–Volmer plot. The K_q values obtained were $1.20 \times 10^5\ M^{-1}$, $2.26 \times 10^5\ M^{-1}$ and $1.22 \times 10^5\ M^{-1}$ for compound **1**, **2** and **3**, respectively. It may be mentioned here that the K_q value obtained for the ligand (compound **1**) was comparatively higher than a similar ligand reported earlier.[17] Likewise, the K_q value obtained for the Cu-complex (compound **3**) in the present study was relatively higher than analogous Cu(II) semicarbazone complexes.[17] The K_q values also seem to suggest that the quenching constant was highest for the the Ni-complex (compound **2**) in comparison to the other compounds.

Plasmid cleavage experiments

Based on the strong propensity of compounds **1–3** to bind to DNA, we were motivated to ascertain the DNA cleavage activity of the compounds. To this end, varying concentrations of compounds **1–3** (60 μM and 180 μM) were interacted with 60 μM purified pUC18 plasmid DNA for varying time periods (1 h and 2 h). The result of the experiments is shown in Fig. S14, ESI†. Topologically different forms of plasmid DNA, namely supercoiled (SC) and nicked circular (NC), were evident in the untreated pUC18 plasmid (Fig. S14 A–D, Lane 1, ESI†). When the pUC18 plasmid DNA was treated with a concentration of 60 μM of compounds **1–3**, DNA cleavage activity could not be detected for any sample (Fig. S14 A–B, ESI†). At a higher concentration of the compounds (180 μM), it was observed that for compound **3**, a stained band was detected in the well of the agarose gel, indicating that the sample failed to migrate during the electrophoretic run (Fig. S14 C–D, lane no. 4, ESI†). The binding of high concentrations of the Cu(II)-complex to DNA may lead to interference in the characteristic mobility of the native DNA under the electrophoretic conditions and consequently, the complex-bound DNA fails to migrate from the well. The interaction of pUC18 plasmid DNA with 180 μM of either the ligand or the Ni(II)-complex did not result in any cleavage activity and the mobility of the plasmid DNA was also unaffected (Fig. S14 C–D, lane nos. 2–3, ESI†).

Protein binding studies

Studies related to the binding of small ligands with BSA are usually examined by fluorescence spectroscopic techniques. The fluorescence of BSA is commonly attributed to two fluorophoric amino acid residues of the protein, namely tryptophan and tyrosine. Changes in the protein conformation, subunit associations, substrate binding or denaturation usually affect the emission pattern of tryptophan. Therefore, the tryptophan fluorescence of BSA can provide structural information of the protein and it can be employed in understanding the protein folding mechanism and association reactions. As the excitation wavelength of tyrosine is less (~280 nm) than the excitation wavelength of tryptophan (~295 nm), thus, the excitation wavelength of 295 nm was chosen to avoid the contribution from any of the tyrosine residues in BSA. We have studied the interaction of BSA with

compounds **1**, **2** and **3** by fluorescence measurements at room temperature. A decrease in the fluorescence intensity of the tryptophan moiety at 346 nm in the order of 75%, 87.55% and 97.03% was observed upon the interaction of BSA with compounds **1**, **2** and **3**, respectively. The diminution of the emission intensity is accompanied by the significant development of a new hump at a red shifted wavelength (Fig. S15, ESI†). The shifting of the emission maxima towards a higher wavelength along with the formation of an iso-emissive point is a clear indication of the probable energy transfer from the indole unit of the tryptophan to the protein bound compounds.

Furthermore, the fluorescence quenching data were studied using the Stern–Volmer equation, a modified Stern–Volmer equation and Scatchard equation. On the basis of the relationship between the quenching of the excited states and the quencher concentration, the Stern–Volmer equation is given by eqn (1). Here, F_0 and F are the relative fluorescence intensities in the absence and presence of quencher, respectively, and [Q] is the concentration of the quencher. K_q is the Stern–Volmer quenching constant, which measures the efficiency of the quenching. In the case of compound **2**, a plot with an upward curvature, concave towards the *y*-axis, was obtained. This type of positive deviation from the Stern–Volmer equation is frequently observed when the extent of the quenching is large and is due to the quenching of the fluorophore by collision and by complex formation with the same quencher.[32] For the above mentioned phenomenon, the Stern–Volmer plot can be analyzed using a modified Stern–Volmer equation, as stated below in eqn (2). The modified Stern–Volmer equation is second order in [Q], which accounts for the upward curvature observed when static and dynamic quenching occur for the same fluorophore.

$$F_0/F = K_{app}\,[Q] + 1 \quad (2)$$

where, $K_{app} = (K_D + K_S) + K_D K_S[Q]$

Here, K_D is the dynamic quenching constant and K_S is the static quenching constant.

The equilibrium binding constant was analyzed using the Scatchard equation (eqn (3)):

$$\log\,[(F_0 - F)/F] = \log K_{bin} + n \log\,[Q] \quad (3)$$

where K_{bin} is the binding constant of the compound with BSA and n is the number of binding sites. The modified Scatchard equation used in the present study is similar to that used in earlier investigations to determine the binding interaction between a protein (BSA) and ligand (or metal complex).[6h,18,33] The number of binding sites (n) and the binding constant (K_{bin}) have been calculated from the plot of log $[(F_0 - F)/F]$ *vs.* log[Q] (Fig. S16, ESI†). The calculated K_q, K_{app} and K_{bin} values of compounds **1**, **2** and **3** are given in Table 4. These values are in general agreement with the K values reported in the literature for analogous protein–ligand or protein–metal complex interactions.[6h,18,33]

Generally, quenching of the emission intensity of a fluorophore occurs by either dynamic or static quenching mechanisms. In a typical dynamic quenching, the fluorophore and the quencher come into contact during the transient presence of the excited state, while in case of static quenching, fluorophore–quencher complex formation occurs in the ground state. One of the simple and decisive methods to differentiate between static and dynamic quenching is UV-visible absorption spectroscopy. The UV-visible spectra of BSA with the incremental addition of compounds **1**, **2** and **3** show an increase in the absorption intensity of BSA as compounds **1**, **2** and **3** are added (Fig. S17, ESI†). The significant changes observed in the UV-visible spectra of BSA clearly suggest that fluorophore–quencher complex formation is occurring in the ground state for compound **1** and **3**, wherein static quenching is exclusively occurring. In the case of compound **2**, the combined results from the UV-visible and fluorescence experiments indicate that static quenching of BSA occurs in the presence of compound **2** along with an adequate contribution from collision/dynamic quenching.

Distance measurement using resonance energy transfer between quenchers and BSA

The FRET (Fluorescence Resonance Energy Transfer) technique has emerged as a successful tool to determine the spatial distance between a donor and an acceptor in proteins and FRET distances have been extensively used to study protein folding pathways, conformational changes upon ligand binding, protein–protein interactions and monomer–dimer equilibria.[34] According to Förster's theory, the efficiency of FRET depends mainly on the following factors: (i) the extent of the overlap between the donor emission and the acceptor absorption, (ii) the orientation of the transition dipole of the donor and acceptor, and (iii) the distance between the donor and the acceptor.[35] In a proteinaceous environment, the proximity of a guest molecule to the tryptophan moiety is often determined through a FRET study. For this purpose, the donor (BSA) was excited at 295 nm, where the absorbance of the acceptors (ligands) was negligible. On the gradual addition of guest molecules, the fluorescence intensity of the tryptophan residue present in BSA decreased along with the development of a new red shifted hump, which was accompanied by the

Table 4 Quenching and energy transfer parameters of different BSA–compound composites

	Stern–Volmer constant (K_q or K_{app})	Binding constant (K_{bin})	R_0 (nm)	E
L	$8.3 \times 10^4\ M^{-1}$	$1.4 \times 10^4\ M^{-1}$	2.49	0.75
L–Ni Complex	$1.8 \times 10^5\ M^{-1}$ (K_{app})	$4.2 \times 10^5\ M^{-1}$	3.09	0.87
L–Cu Complex	$1.2 \times 10^5\ M^{-1}$	$2.5 \times 10^5\ M^{-1}$	2.43	0.80

formation of a distinct iso-emissive point (Fig. S15, ESI†). Taken together, this result indicates that the quenching of the tryptophan fluorescence may be due to a non-radiative energy transfer between the tryptophan and the guest molecules. As per Förster's theory, the efficiency of the energy transfer (E) is related to the distance r between the donor and acceptor by the following equation:

$$E = R_0^6/(R_0^6 + r^6) \quad (4)$$

where r is the distance between the acceptor and donor and R_0 is the critical distance when the transfer efficiency is 50% and is given by the following equation:

$$R_0 = 0.211[\kappa^2\, n^{-4}\, \Phi_D\, J(\lambda)]^{1/6} \quad (5)$$

where n is the refractive index of the medium, κ^2 is the orientation factor and Φ_D is the quantum yield of the donor. The spectral overlap integral (J) between the donor emission spectrum and the acceptor absorbance spectrum was approximated by the following summation:

$$J(\lambda) = \int F_d(\lambda)\varepsilon_a(\lambda)\lambda^4 d\lambda / \int F_d(\lambda) d\lambda \quad (6)$$

where $F_d(\lambda)$ and $\varepsilon_a(\lambda)$ represent the fluorescence intensity of the donor and the molar extinction coefficient of the acceptor, respectively, at the wavelength λ. The value of J can be evaluated by integrating the overlapped portion of the spectra in Fig. 5 and Fig. S18 (ESI†). If both the donor and acceptor are tumbling rapidly and free to assume any orientations, then the dipole orientation factor, κ^2, equals 2/3.[36a] In the present case, n = 1.36 and Φ_D = 0.118.[36] The energy transfer data were obtained by measuring the change in donor fluorescence. The donor fluorescence intensity (F_d) was measured in the absence and presence (F_a) of acceptor. The efficiency of transfer (E) was calculated using

$$E = 1 - F_a/F_d \quad (7)$$

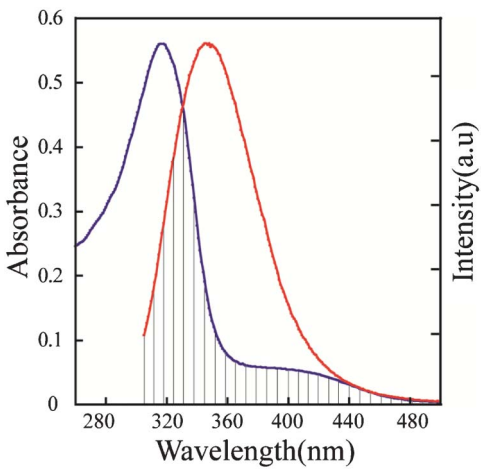

Fig. 5 The overlap of the fluorescence spectra of BSA (red line) and the absorption spectra of compound **1** (blue line).

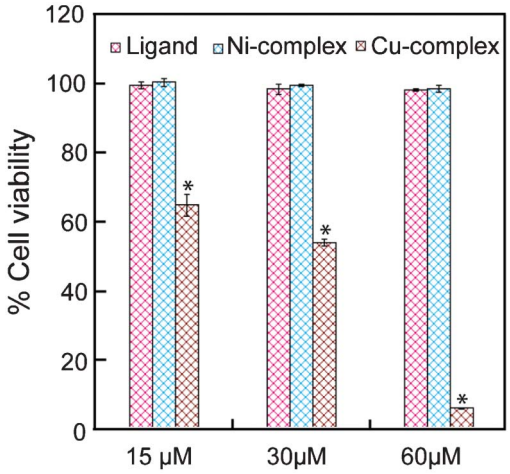

Fig. 6 MTT-based cell viability assay of the compounds on HeLa cell lines after 24 h incubation. * indicates a p value < 0.001 in ANOVA.

The calculated values of R_0 and E using Förster's theory are presented in Table 4.

Cytotoxicity assay

Based on the premise that the test compounds displayed an appreciable interaction with biological macromolecules, such as DNA and proteins, it was pertinent to investigate the cytotoxic effect of these compounds on model human cell lines. As evident from Fig. 6, the ligand as well as the Ni(II)-complex failed to exert any cytotoxic effect on human cervical carcinoma (HeLa) cell lines. In contrast, the Cu(II)-complex revealed a dose-dependent cytotoxic effect, with an IC_{50} value of 31.27 μM (Fig. S19, ESI†). It can be mentioned here that the viability of cells treated with the Cu(II)-complex was significantly low (p value < 0.001 based on ANOVA) compared to the viability observed in the case of cells treated with the ligand or Ni(II)-complex. The anti-proliferative effect of the Cu-complex against HeLa cells indicates that the complex has the potential to act as an anti-cancer chemotherapeutic agent. There are reports which suggest that Cu(II) complexes are cytotoxic and this phenomenon has been attributed to their DNA cleavage activity.[37] However, in the present study, it was observed that the Cu(II)-complex failed to display any DNA cleavage activity even at a concentration of 60 μM (Fig. S14A–B, ESI†). These results suggest that in the case of the Cu(II)-complex, the observed cytotoxicity is probably attributed to a mechanism other than DNA cleavage and warrants further investigation.

Conclusions

In summary, a new pyridine-based thiosemicarbazone ligand LH and its Cu(II) and Ni(II) complexes have been synthesized and characterized by structural, analytical and detailed spectroscopic methods. The results of DNA binding experi-

ments revealed that the free ligand and its Ni(II) and Cu(II) complexes significantly bind to double stranded DNA, possibly by intercalation. Their interactions with plasmid DNA and agarose gel electrophoresis suggested that none of the complexes could induce DNA cleavage, although the Cu(II) complex was able to strongly bind to DNA and interfere with its electrophoretic mobility. The protein binding studies of the compounds suggested a static quenching interaction with BSA for compound **1** and **3** whereas the fluorescence quenching of BSA in the presence of compound **2** was a combined effect of both static and collision/dynamic quenching processes. Interestingly, the fluorescence quenching of BSA in the presence of compounds **1**, **2** and **3** was due to the spectral overlap between the donor's fluorescence and acceptor's absorption, suggesting the quenching of the fluorescence of BSA is attributed to an energy transfer process from the tryptophan residues to the BSA bound compounds. Amongst the test compounds, only the Cu-complex displayed prominent cytotoxic activity against HeLa cells. This compound holds promise as an anti-cancer chemotherapeutic agent and in future studies, our endeavour would be to unravel the mechanism of the cytotoxic activity of this compound.

Acknowledgements

G. D. acknowledges the Council of Scientific and Industrial Research (EMR/01/3664/12) and the Department of Science and Technology (DST), New Delhi, India for financial support, CIF and IIT Guwahati for providing instrument facilities and DST FIST for the single crystal X-ray diffraction facility. A. R thanks the Department of Biotechnology (DBT), Government of India, for a research grant (BT/01/NE/PS/08). A. B, D. T and C. K are thankful to IIT Guwahati for a research fellowship. We are also thankful to Debraj Biswas for his kind cooperation.

References

1 (*a*) D. R. Richardson, *Crit. Rev. Oncol./Hematol.*, 2002, **42**, 267; (*b*) P. Jutten, W. Schumann, A. Hartl, L. Heinisch, U. Grafe, W. Werner and H. Ulbricht, *Bioorg. Med. Chem. Lett.*, 2002, **12**, 1339.

2 (*a*) J. S. Casas, M. S. Garcıa-Tasende and J. Sordo, *Coord. Chem. Rev.*, 2000, **209**, 197–261; (*b*) T. S. Lobana, R. Sharma, G. Bawa and S. Khanna, *Coord. Chem. Rev.*, 2009, **253**, 977–1055; (*c*) A. Basu and G. Das, *Inorg. Chim.Acta.*, 2011, **372**, 394–399.

3 A. G. Quiroga and C. Navarro-Ranninger, *Coord. Chem. Rev.*, 2004, **248**, 119–133.

4 (*a*) C. Q. Debra, A. K. Kathy and R. K. Earl, *Antiviral Res.*, 2006, **71**, 24–30; (*b*) W. F. T. McMath and H. T. H. Wilson, *Br Med J.*, 1956, **1**, 1041–1042; (*c*) C. E. Van Rooyen, J. Casey, S. H. Lee, R. Faulkner and H. P. Dincsoy, *Can Med Assoc J.*, 1967, **97**, 160–165; (*d*) D. C. Hutfield and G. W. Csonka, *Lancet*, 1964, **1**, 329–330; (*e*) A. M. Tsimberidou, Y. Alvarado and F. J. Giles, *Expert Rev Anticancer Ther*, 2002, **2**, 437–448.

5 (*a*) Y. Teitz, D. Ronen, A. Vansover, T. Stematsky and J. L. Riggs, *Antiviral Res.*, 1994, **24**, 305–314; (*b*) M. C. R. Arguelles, E. C. L. Silva, J. Sanmartın, P. Pelagatti and F. Zani, *J. Inorg. Biochem.*, 2005, **99**, 2231–2239.

6 (*a*) R. Prabhakaran, V. Krishnan, K. Pasumpon, D. Sukanya, E. Wendel, C. Jayabalakrishnan, H. Bertagnolli and K. Natarajan, *Appl. Organomet. Chem.*, 2006, **20**, 203–213; (*b*) R. Prabhakaran, R. Huang, R. Karvembu, C. Jayabalakrishnan and K. Natarajan, *Inorg. Chim. Acta*, 2007, **360**, 691–694; (*c*) R. Prabhakaran, R. Huang, S. V. Renukadevi, R. Karvembu, M. Zeller and K. Natarajan, *Inorg. Chim.Acta*, 2008, **361**, 2547–2552; (*d*) R. Prabhakaran, S. Anantharaman, M. Thilagavathi, M. V. Kaveri, P. Kalaivani, R. Karvembu, N. Dharmaraj, H. Bertagnolli and K. Natarajan, *Spectrochim. Acta, Part A*, 2011, **78**, 844–853; (*e*) R. Prabhakaran, P. Kalaivani, R. Jayakumar, M. Zeller, A. D. Hunter, S. V. Renukadevi, E. Ramachandran and K. Natarajan, *Metallomics*, 2011, **3**, 42–48; (*f*) R. Prabhakaran, P. Kalaivani, R. Huang, M. Sieger, W. Kaim, P. Viswanathamurthi, F. Dallemer and K. Natarajan, *Inorg. Chim. Acta*, 2011, **376**, 317–324; (*g*) P. Kalaivani, R. Prabhakaran, E. Ramachandran, F. Dallemer, G. Paramaguru, R. Renganathan, P. Poornima, V. V. Padma and K. Natarajan, *Dalton Trans.*, 2012, **41**, 2486–2499; (*h*) R. Prabhakaran, P. Kalaivani, P. Poornima, F. Dallemer, G. Paramaguru, V. Vijaya Padma, R. Renganathan, R. Huange and K. Natarajan, *Dalton Trans.*, 2012, **41**, 9323–9336.

7 M. C. R. Arguelles, E. C. L. Silva, J. Sanmartın, A. Bacchi, C. Pelizzi and F. Zani, *Inorg. Chim.Acta*, 2004, **357**, 2543–255.

8 A. Cukurovali, I. Yilmaz, S. Gur and C. Kazaz, *Eur. J. Med. Chem.*, 2006, **41**, 201–207.

9 A. Murugkar, B. Unnikrishnan, S. Padhye, R. Bhonde, S. Teat, E. Triantafillou and E. Sinn, *Met.-Based Drugs*, 1999, **6**, 177–182.

10 Y. Teitz, N. Barko, M. Abramoff and D. Ronen, *Chemotherapy*, 1994, **40**, 195–200.

11 W. X. Hu, W. Zhou, C. Xia and X. Wen, *Bioorg. Med. Chem. Lett.*, 2006, **16**, 2213–2218.

12 Z. Afrasiabi, E. Sinn, S. Padhye, S. Dutta, S. Padhye, C. Newton, C. E. Anson and A. K. Powell, *J. Inorg. Biochem.*, 2003, **95**, 306–314.

13 T. Bal, B. Atasever, Z. Solakoglu, S. E. Kuruca and B. Ulkuseven, *Eur. J. Med. Chem.*, 2007, **42**, 161–167.

14 M. Campana, C. Laborie, G. Barbier, R. Assan and R. Milcent, *Eur. J. Med. Chem.*, 1991, **26**, 273–278.

15 (*a*) R. Noto, F. Buccheri, G. Cusmano, M. Gruttadauria and G. J. Werber, *J. Heterocycl. Chem.*, 1991, **28**, 1421–1427; (*b*) R. Noto, P. Lo Meo, M. Gruttadauria and G. Werber, *J. Heterocycl. Chem.*, 1999, **36**, 667–674; (*c*) S. Buscemi and M. Gruttadauria, *Tetrahedron*, 2000, **56**, 999–1004; (*d*) M. H. Shih and C. L. Wu, *Tetrahedron*, 2005, **61**, 10917–10925; (*e*) J. P. Kilburn, J. Lau and R. C. F. Jones, *Tetrahedron Lett.*, 2003, **44**, 7825–7828; (*f*) R. Severinsen, J. P. Kilburn and J. F. Lau, *Tetrahedron*, 2005, **61**, 5565–5575; (*g*) E. Lopez-Torres, A. R. Cowley and J. R. Dilworth, *Dalton Trans.*, 2007, 1194–1196; (*h*) A. Basu and G. Das, *Dalton Trans.*, 2011, **40**, 2837–2843.

16 (*a*) D. Senthil Raja, G. Paramaguru, N. S. P. Bhuvanesh, J. H. Reibenspies, R. Renganathan and K. Natarajan, *Dalton Trans.*, 2011, **40**, 4548–4559; (*b*) D. Senthil Raja, N. S. P. Bhuvanesh and K. Natarajan, *Eur. J. Med. Chem.*, 2011, **46**, 4584–4594; (*c*) E. Ramachandran, P. Kalaivani, R. Prabhakaran, M. Zeller, J. H. Bartlett, P. O. Adero, T. R. Wagner and

K. Natarajan, *Inorg. Chim. Acta*, 2012, **385**, 94–99; (*d*) E. Ramachandran, S. P. Thomas, P. Poornima, P. Kalaivani, R. Prabhakaran, V. V. Padma and K. Natarajan, *Eur. J. Med. Chem.*, 2012, **50**, 405–415.

17 D. S. Raja, N. S. P. Bhuvanesh and K. Natarajan, *Inorg. Chem.*, 2011, **50**, 12852–12866.

18 E. Ramachandran, D. S. Raja, J. L. Mike, T. R. Wagner, M. Zellerb and K. Natarajan, *RSC Adv.*, 2012, **2**, 8515–8525.

19 (*a*) F. Mancin, P. Scrimin, P. Tecilla and U. Tonellato, *Chem. Commun.*, 2005, 2540; (*b*) R. Pitie, C. J. Burrows and B. Meunier, *Nucleic Acids Res.*, 2000, **28**, 4856; (*c*) B. Maity, M. Roy, S. Saha and A. R. Chakravarty, *Organometallics*, 2009, **28**, 1495; (*d*) J. A. Cowan and A. Sreedhara, *JBIC, J. Biol. Inorg. Chem.*, 2001, **6**, 337; (*e*) N. H. Williams, B. Takasaki, M. Wall and J. Chin, *Acc. Chem. Res.*, 1999, **32**, 485; (*f*) D. S. Sigman, A. Mazumder and D. M. Perrin, *Chem. Rev.*, 1993, **93**, 2295; (*g*) R. Tawa, D. Gao, M. Takami, Y. Imakura, K.-H. Lee and H. Sakurai, *Bioorg. Med. Chem.*, 1998, **6**, 1003; (*h*) M. E. Branum, A. K. Tipton, S. Zhua and L. Jr. Que, *J. Am. Chem. Soc.*, 2001, **123**, 1898; (*i*) J.-C. Francois, T. Saison-Behmoaras, C. Barbier, M. Chassignol, N. T. Thuong and C. Héléne, *Proc. Natl. Acad. Sci. U. S. A.*, 1989, **86**, 9702; (*j*) M. P. Fitzsimons and J. K. Barton, *J. Am. Chem. Soc.*, 1997, **119**, 3379; (*k*) R. Hettich and H.-J. Schneider, *J. Am. Chem. Soc.*, 1997, **119**, 5638; (*l*) B. C. Bales, M. Pitié, B. Meunier and M. A. Greenberg, *J. Am. Chem. Soc.*, 2002, **124**, 9062.

20 (*a*) S. A. Khan, *Eur. J. Med. Chem.*, 2008, **43**, 2040–2044; (*b*) S. Dutta, S. Padhye, K. I. Priyadarsini and C. Newton, *Bioorg. Med. Chem. Lett.*, 2005, **15**, 2738–2744; (*c*) R. B. d. Oliveira, E. M. d. Souza-Fagundes, R. P. P. Soares, A. A. Andrade, A. U. Krettli and C. L. Zani, *Eur. J. Med. Chem.*, 2008, **43**, 1983–1988; (*d*) H. Cerecetto, R. D. Maio, M. Gonzalez, M. Risso, G. Sagrera, G. Seoane, A. Denicola, G. Peluffo, C. Quijano, A. O. M. Stoppani, M. Paulino, C. Olea-Azar and M. A. Basombrio, *Eur. J. Med. Chem.*, 2000, **35**, 343–350; (*e*) J. R. Dimmock, R. N. Puthucode, J. M. Smith, M. Hetherington, J. W. Quail, U. Pugazhenthi, T. Lechler and J. P. Stables, *J. Med. Chem.*, 1996, **39**, 3984–3997; (*f*) J. R. Dimmock, S. N. Pandeya, J. W. Quail, U. Pugazhenthi, T. M. Allen, G. Y. Kao, J. Balzarini and E. Declercq, *Eur. J. Med. Chem.*, 1995, **30**, 303–314.

21 (*a*) B. Ojha and G. Das, *J. Phys. Chem. B*, 2010, **114**, 3979–3986; (*b*) B. Ojha and G. Das, *Chem. Commun.*, 2010, **46**, 2079–2081; (*c*) B. Ojha and G. Das, *Photochem. Photobiol. Sci.*, 2011, **10**, 554–56; (*d*) B. Ojha and G. Das, *Chem. Phys. Lipids*, 2011, **164**, 144–150; (*e*) C. Kar, B. Ojha and G. Das, *Luminescence*, 2013, **28**, 339–344.

22 *SAINT, SMART and XPREP*, Siemens Analytical X-ray Instruments Inc.: Madison, WI, 1995.

23 G. M. Sheldrick, *SADABS: Software for Empirical Absorption Correction*, University of Göttingen, Institute fur Anorganische Chemieder Universitat, Göttingen, Germany, 1999–2003.

24 (*a*) G. M. Sheldrick, *SHELXS-97*, University of Göttingen, Göttingen,Germany, 1997; (*b*) G. M. Sheldrick, *SHELXL 97, Program for Crystal Structure Refinement*, University of Göttingen, Göttingen, Germany, 1997.

25 *Mercury 2.3, supplied with Cambridge Structural Database, CCDC*, Cambridge, U. K., 2003–2004.

26 J. Nath, B. K. Patel, L. Jamir, S. U. Bora and K. V. V. V. Satyanarayana, *Green Chem.*, 2009, **11**, 1503–1506.

27 M. Joseph, M. Kuriakose, M. R. P. Kurupa, E. Suresh, A. Kishore and S. G. Bhat, *Polyhedron*, 2006, **25**, 61–70.

28 (*a*) Z. C. Liu, B. D. Wang, Z. Y. Yang, Y. Li, D. D. Qin and T. R. Li, *Eur. J. Med. Chem.*, 2009, **44**, 4477–4484; (*b*) Z. C. Liu, B. D. Wang, B. Li, Q. Wang, Z. Y. Yang, T. R. Li and Y. Li, *Eur. J. Med. Chem.*, 2010, **45**, 5353–5361.

29 (*a*) E. C. Long and J. K. Barton, *Acc. Chem. Res.*, 1990, **23**, 271–273; (*b*) H. F. Wang, R. Shen and N. Tang, *Eur. J. Med. Chem.*, 2009, **44**, 4509–4515.

30 D. S. Raja, N. S. P. Bhuvanesh and K. Natarajan, *Eur. J. Med. Chem.*, 2011, **46**, 4584–4594.

31 Y. B. Zeng, N. Yang, W. S. Liu and N. Tang, *J. Inorg. Biochem.*, 2003, **97**, 258–264.

32 J. R. Lakowicz, *Principles of Fluorescence Spectroscopy*, 2nd ed., Kluwer Academic/Plenum Publishers: New York, 1999.

33 (*a*) J.-Q. Lu, F. Jin, T.-Q. Sun and X.-W. Zhou, *Int. J. Biol. Macromol.*, 2007, **40**, 299–304; (*b*) F. Zhang, Q.-Y. Lin, S.-K. Li, Y.-L. Zhao, P.-P. Wang and M.-M. Chen, *Spectrochim. Acta, Part A*, 2012, **98**, 436–443.

34 (*a*) M. Dockal, M. Chang, D. C. Carter and F. Ruker, *Protein Sci.*, 2000, **9**, 1455–1465; (*b*) A. A. Deniz, T. A. Laurence, G. S. Beligere, M. Dahan, A. B. Martin, D. S. Chemla, P. E. Dawson, P. G. Schultz and S. Weiss, *Proc. Natl. Acad. Sci. U. S. A.*, 2000, **97**, 5179–84; (*c*) J. Mukhopadhyay, A. N. Kapanidis, V. Mekler, E. Kortkhonjia, Y. W. Ebright and R. H. Ebright, *Cell*, 2001, **106**, 453–63.

35 R. Mukherjee, *KK, Fundamentals of Photochemistry*, Wiley Eastern: New Delhi, 1986.

36 (*a*) T. Förster, *Discuss. Faraday Soc.*, 1959, **27**, 7–17; (*b*) T. Sen, K. K. Haldar and A. Patra, *J. Phys. Chem. C*, 2008, **112**, 17945–17951.

37 (*a*) P. Jaividhya, R. Dhivya, M. A. Akbarsha and M. Palaniandavar, *J. Inorg. Biochem.*, 2012, **114**, 94–105; (*b*) C. Marzano, M. Pellei, F. Tisato and C. Santini, *Anti-Cancer Agents Med. Chem.*, 2009, **9**, 185–211.

